Published online 9 January 2023

Nucleic Acids Research, 2023, Vol. 51, No. 3 ***1245–1259***
https://doi.org/10.1093/nar/gkac1219

Alternative splicing mediates the compensatory upregulation of MBNL2 upon MBNL1 loss-of-function

Larissa Nitschke[1], Rong-Chi Hu[1,2], Andrew N. Miller[1], Lathan Lucas[1,3] and Thomas A. Cooper[1,2,4,*]

[1]Department of Pathology & Immunology, Baylor College of Medicine, Houston, TX 77030, USA, [2]Department of Molecular Physiology & Biophysics, Baylor College of Medicine, Houston, TX 77030, USA, [3]Chemical, Physical & Structural Biology Graduate Program, Baylor College of Medicine, Houston, TX 77030, USA and [4]Department of Molecular & Cellular Biology, Baylor College of Medicine, Houston, TX 77030, USA

Received October 22, 2022; Revised December 05, 2022; Editorial Decision December 06, 2022; Accepted January 03, 2023

ABSTRACT

Loss of gene function can be compensated by paralogs with redundant functions. An example of such compensation are the paralogs of the Muscleblind-Like (MBNL) family of RNA-binding proteins that are sequestered and lose their function in Myotonic Dystrophy Type 1 (DM1). Loss of MBNL1 increases the levels of its paralog MBNL2 in tissues where *Mbnl2* expression is low, allowing MBNL2 to functionally compensate for MBNL1 loss. Here, we show that loss of MBNL1 increases the inclusion of *Mbnl2* exon 6 and exon 9. We find that inclusion of *Mbnl2* exon 6 increases the translocation of MBNL2 to the nucleus, while the inclusion of *Mbnl2* exon 9 shifts the reading frame to an alternative C-terminus. We show that the C-terminus lacking exon 9 contains a PEST domain which causes proteasomal degradation. Loss of MBNL1 increases the inclusion of exon 9, resulting in an alternative C-terminus lacking the PEST domain and the increase of MBNL2. We further find that the compensatory mechanism is active in a mouse DM1 model. Together, this study uncovers the compensatory mechanism by which loss of MBNL1 upregulates its paralog MBNL2 and highlights a potential role of the compensatory mechanism in DM1.

INTRODUCTION

Genetic robustness is the ability of an organism to maintain its reproductive fitness despite harmful genetic perturbations (1–4). This robustness can arise from redundant genes, such as paralogs, with overlapping functions and temporospatial expression that can compensate for gene loss (3–5). Loss of a single paralog thereby results in no or only minor phenotypic consequences, whereas loss of both paralogs leads to severe phenotypes and lethality (3,5). While the phenomenon of paralog compensation has been widely observed, the underlying molecular mechanisms and roles in preventing or modifying disease severity remain poorly understood.

An example of paralog compensation is found with the paralogs of the Muscleblind-Like (MBNL) family of RNA-binding proteins, key regulators of RNA processing, including alternative splicing, alternative polyadenylation, RNA stability, and RNA subcellular localization (6,7). The MBNL paralogs are involved in the multisystemic disorder Myotonic Dystrophy Type 1 (DM1), the most common cause of adult-onset muscular dystrophy, clinically affecting 1:8500 individuals (8–11). DM1 is caused by a CTG repeat expansion in the 3' untranslated region (3' UTR) of the Dystrophia Myotonica Protein Kinase (*DMPK*) gene (12–14). The CTG repeats in the mutant *DMPK* allele are highly unstable and undergo somatic and intergenerational expansions (15–17). The RNA transcribed from the expanded *DMPK* allele contains tracts of CUG repeats (CUGexp RNA) that form stem-loop structures with high affinity for MBNL proteins that sequester the MBNL paralogs, causing their loss of function and leading to the dysregulation of RNA processing (8,9,18).

The MBNL family consists of three paralogs that are highly conserved in structure and function (6,19). *Mbnl1* is widely expressed and the predominant paralog in muscle and heart, while *Mbnl2* expression is enriched in the brain (6,7,20). *Mbnl3* is expressed primarily during embryonic development and in the placenta but is barely detectable in most other adult tissues (6,21,22). Interestingly, while MBNL1 is the predominant paralog in muscle and heart, $Mbnl1^{-/-}$ mice display relatively mild and partial DM1-associated phenotypes (23). In contrast, compound knockout of *Mbnl1* and *Mbnl2* results in severe DM1-related phenotypes in heart and muscle, including cardiac arrhythmias and conduction block, severe myotonia, skeletal muscle weakness, and reduced lifespan (7). These results indicate a functional compensation of the MBNL paralogs and raise

*To whom correspondence should be addressed. Tel: +1 713 798 3141; Email: tcooper@bcm.edu

the question of how MBNL2 compensates for the loss of MBNL1 in tissues where its expression is relatively low. Previous work revealed that loss of MBNL1 increases MBNL2 protein levels, which, in turn, allows MBNL2 to bind to MBNL1-regulated target genes and compensate for the loss of MBNL1 (7,24). The mechanism behind the compensatory upregulation of MBNL2 and its importance in DM1 remains unknown.

In this study, we generated *Mbnl1*$^{-/-}$ mice and confirmed previous studies showing an increase in MBNL2 protein levels in muscle and heart and, to a lesser extent, in brain. We found that loss of MBNL1 increases the inclusion of two alternative exons in *Mbnl2,* exon 6 and exon 9. Inclusion of *Mbnl2* exon 6 introduces a nuclear localization signal (NLS) and increases the translocation of MBNL2 to the nucleus, while inclusion of *Mbnl2* exon 9 increases MBNL2 protein levels. Due to its size of 95bp, inclusion of exon 9 results in a frameshift that produces an alternative C-terminus in MBNL2, removing a PEST degradation domain in the C-terminus encoded by the mRNA that excludes exon 9. We also found that inclusion of *Mbnl2* exon 6 and exon 9 and MBNL2 protein levels are significantly increased in our inducible DM1 heart mouse model (CUG960) that expresses an mRNA containing 960 CUG repeats in the context of human *DMPK* (25), indicating that the compensatory mechanism might also be active in DM1 tissues.

MATERIALS AND METHODS

Mouse husbandry

All mice were housed and maintained in the animal facilities at Baylor College of Medicine. The mice were kept on a 12 h light/dark cycle. Animal care and experimental procedures were approved by the institutional animal care and use committee of Baylor College of Medicine, according to the US National Institutes of Health Guidelines.

Generation of *Mbnl1* knockout mouse model

Mbnl1$^{flox/flox}$ mice were generated via CRISPR/Cas9-mediated gene editing using two gRNAs targeting regions upstream and downstream of the 1049 bp *Mbnl1* exon 3 (26,27). The 5′gRNA (5′-CCTTATTCTCGACACAAGACCTC-3′) and the 3′gRNA (5′-GCCCTGTATCAGGTTTCAAGTGG-3′) were designed using the sanger.ac.uk homepage and purchased from Synthego (28). Single-stranded oligonucleotide (ssODN) for the 5′LoxP site (5′-CTTAATAA TTAATGTTCCTGCAATGGAATCGCTTTCTCCCTG GAGGTTGGCTTTCAGATTTACCAGACATCTGA CAACACTGCACCCCTTACTCGAGATAACTTCGTA TAGCATACATTATACGAAGTTATTTCTCGACACA AGACCTCAGCTTCTGCTTTAAGAAAC-3′) and the 3′LoxP site (5′-ATCAAGCAGGTTGAAGACACCCCA GAACACATTTCTAGCCTTGACCTTGTATCAAAAC AAAGACATGTGTGCTATCTTTACAAGACCCAC TATAACTTCGTATAATGTATGCTATACGAAGTTA TCTCGAGTGAAACCTGATACAGGGCTTACAAG TCCAATGACAGT-3′) were purchased from IDT for homologous-directed recombination to introduce the LoxP sites upstream and downstream of *Mbnl1* exon 3.

Female C57BL/6NJ WT mice at the age of three to five weeks were super-ovulated via injection of 5 IU of PMSG (Thermo Fisher) and 47 hrs later with 5 IU HCG (Thermo Fisher) in 0.9% NaCl. Upon overnight breeding with C57BL/6NJ WT males, the females' ova were dissected. An injection mixture containing 30 ng/ul Cas9 protein (PNA Bio), 20 ng/ul sgRNA and 40 ng/ul ssODN in 10 mM Tris pH 7.5 and 0.25 mM EDTA was prepared, and about 2 pl was injected into the pronucleus of extracted ova. The ova were then transferred into oviducts of pseudo-pregnant ICR (CD1) females by the Baylor College of Medicine Genetically Engineered Mouse Core.

Upon birth, the mice were genotyped to distinguish the unmodified (WT) and modified LoxP alleles. For the 5′LoxP site the following primers were used: Mbnl1_5LoxP_For (5′-TGTTCCTGCAATGGAATCGC-3′) and Mbnl1_5LoxP_Rev (5′-GGCGAGGGATGA ACAAAAGC-3′). The expected band sizes for the WT product were 151 bp and for the LoxP product 191 bp. For the 3′LoxP site the following primers were used: Mbnl1_3LoxP_For (5′-AAGTTAGCCT TGTGTGTGTGA-3′) and Mbnl1_3LoxP_Rev (5′-AAGCAGGTTGAAGACACCCC-3′). The expected band sizes for the WT product were 192 bp and for the LoxP product 232 bp. Positive founders were backcrossed to C57BL/6NJ WT animals, and the correct sequence of the F1 offspring was confirmed using Sanger sequencing (Genewiz).

The *Mbnl1*$^{flox/flox}$ line was backcrossed to C57BL/6NJ WT animals for over six generations starting with a sequence-verified F1 animal. To generate *Mbnl1*$^{+/-}$ mice, *Mbnl1*$^{flox/+}$ embryos were incubated with Cre Recombinase (Excellgen) and transferred into pseudo-pregnant ICR (CD1) (29). The resulting mice were genotyped using the primers Mbnl1_5′LoxP_For and Mbnl1_3′LoxP_Rev. The expected band sizes for the knockout product in the mice with correct Cre recombination was 207 bp. *Mbnl1*$^{+/-}$ mice were crossed to generate the experimental *Mbnl1*$^{+/+}$ (WT) and *Mbnl1*$^{-/-}$ mice.

Protein extraction and western blot from mouse tissues

Homogenates of brain (posterior cortex), skeletal muscle (gastrocnemius muscle), and heart (left ventricle) from 8-week old mice were prepared by homogenization in 1× RIPA buffer (Cell Signaling Technology) supplemented with 1× protease inhibitor (GenDepot) and 1× phosphatase inhibitor (GenDepot). The tissues were mixed with RIPA buffer and 0.10 g of 1.0 mm diameter Zirconium Oxide Beads (Next Advance) and blended with the Bullet Blender 2.4 Tissue Homogenizer (Next Advance). The samples were incubated for 15 min at 4°C and then spun down at 13 000 rpm for 15 min at 4°C. Protein concentrations of the supernatant were measured using the Pierce BCA Protein Assay Kit (Thermo Fisher Scientific). Samples were diluted and prepared in NuPAGE sample reducing agent (Invitrogen) and NuPAGE LDS Sample Buffer (Invitrogen). The samples were then boiled for 10 min and run on a 4–20% Criterion TGX Stain-Free Precast Protein Gel (Bio-Rad Laboratories) in Tris/Glycine/SDS Running Buffer (Bio-Rad Laboratories). The proteins were

Table 1. List of primers used for RT-qPCRs in mouse tissues and cell lines

Name	Sequence
*mMbnl1*_For	CACAGAAGTTAATGCGGACAG
*mMbnl1*_Rev	AGGATGAGCAAACCGACAG
*mMbnl2*_For	CCAGCTAGAGATTAATGGGAGG
*mMbnl2*_Rev	CCGCATTTGTCCCTATGGTG
m*Gapdh*_For	AGGTCGGTGTGAACGGATTTG
m*Gapdh*_Rev	TGTAGACCATGTAGTTGAGGTCA

subsequently transferred to Trans-Blot Turbo Nitrocellulose (Bio-Rad Laboratories) using the Trans-Blot Turbo system (Bio-Rad Laboratories) at 2.5 A, 25 V, 7 min in Trans-Blot Turbo Transfer Buffer (Bio-Rad Laboratories). After blocking for 1 hr at room temperature with 5% Blotto Non Fat Dry-Milk (Chem Cruz) in phosphate buffered saline (10 mM Na_2HPO_4, 2.7 mM KCl, 137 mM NaCl, 1.76 mM KH_2PO_4, pH 7.4) with 0.01% Tween-20 (Sigma-Aldrich) (PBST), membranes were probed overnight at 4°C with anti-MBNL1 (Bethyl Laboratories; 1:1000), anti-MBNL2 (Santa Cruz, 3B4; 1:1000) or anti-vinculin (Sigma-Aldrich, nVIN-1; 1:5000) in 1:1 Odyssey Blocking Buffer PBS (Licor) in PBST. The next day, the blots were washed three times with PBST and incubated for 1 hr at RT in secondary antibody. The secondary antibody used to detect anti-MBNL1 was Horseradish Peroxidase (HRP)-conjugated Rabbit IgG (H&L) Antibody (Jackson Immunoresearch; 1:10 000) in 5% non-fat milk in PBST. The secondary antibody used to detect anti-MBNL2 and anti-vinculin was HRP-conjugated Mouse IgG (H&L) Antibody (Jackson Immunoresearch; 1:10 000) in 5% non-fat milk in PBST. The membranes were then washed three times with PBST, incubated for one minute in West-Q Pico ECL Solution (GenDepot) and then imaged using the ChemiDox MP Imaging System (Bio-Rad).

RNA extraction, RT-qPCR and RT-PCR from mouse tissues

Total RNA was isolated from brain (posterior cortex), skeletal muscle (gastrocnemius muscle) and heart (left ventricle) from 8-week old mouse tissues using the miRNeasy Mini Kit (Qiagen) according to manufacturer instructions. Homogenization was carried out using a Bullet Blender 2.4 Tissue Homogenizer (Next Advance) with 0.1 g of 0.5 mm diameter Zirconium Oxide Beads (Next Advance). Random-primed cDNA was prepared from 1 μg of total RNA using M-MLV Reverse Transcriptase (Invitrogen) according to manufacturer's instructions.

RT-qPCR was performed with PowerUp SYBR Green Master Mix (Applied Biosystems), and samples were run on the CFX Connect Real-time system (Bio-Rad). All samples were analyzed in triplicate and expression of levels of *Mbnl1* and *Mbnl2* were normalized to expression of the housekeeping gene *Gapdh*. Primers for *Mbnl1*, *Mbnl2*, and *Gapdh* were obtained from Sigma-Aldrich (Table 1, Supplemental Table S1).

RT-PCR was performed on cDNA using AmfiSure PCR Master Mix (GenDepot). Samples were run on a 5% polyacrylamide gel (0.1 M Tris, 0.1 M Boric Acid, 2 mM EDTA, 5% acrylamide/bis 19:1 (BIO-RAD), 0.1% APS, 0.18% TEMED (Bio-Rad) in TBE running buffer (0.1 M Tris, 0.1 M Boric Acid, 2 mM EDTA)). The gels were incubated in 0.4 μg/mL Ethidium Bromide in 0.5X TBE for 15 min and imaged using Gel Logic 2200 Imaging System (Kodak). Primers for *Mbnl2* exon 6 and exon 9 were obtained from Sigma-Aldrich (Table 2, Supplemental Tables 2 and 3).

Table 2. List of primers used for RT-PCRs in mouse tissues and cell lines

Name	Sequence
*mMbnl2*_exon5_For	GCAGGCCAAAATCAAAGCTG
*mMbnl2*_exon7_Rev	GCACTGGTCAGAGCCTGC
*mMbnl2*_exon7_For	GGGTGCTCTTCATCCCTTACC
*mMbnl2*_exon10_Rev	GCAGATTCTTGGCATTCCATTCC

Cloning of MBNL2 and mCherry constructs

FLAG-MBNL2(+E9), FLAG-MBNL2(–E9), FLAG-MBNL2(+E6) and FLAG-MBNL2(–E6) constructs were amplified from cDNA using Q5 Hot Start High Fidelity Polymerase (New England Biolabs) and then cloned into the pcDNA3.1 (Invitrogen) vector digested with NotI restriction enzyme using InFusion Snap Assembly Eco Dry (Takara Bio).

FLAG-MBNL2(+E9), FLAG-MBNL2(–E9), FLAG-MBNL2(+E6) and FLAG-MBNL2(–E6) constructs were further amplified from the generated pcDNA3.1 vectors and FLAG-mCherry from pcDNA3.1-mCherry (Addgene #128744) using Q5 Hot Start High Fidelity Polymerase (New England Biolabs) and cloned into the pBi-Tet-On vector (Clonetech) digested with NheI and NotI (New England Biolabs) using InFusion Snap Assembly Eco Dry (Takara Bio).

FLAG-mCherry constructs were amplified from pcDNA3.1-mCherry (Addgene #128744) and the C-termini of MBNL2 from the pBi-Tet-On FLAG-MBNL2(+E9) and FLAG-MBNL2(–E9) constructs and then cloned into pcDNA3.1 (Invitrogen) digested with NotI restriction enzyme using InFusion Snap Assembly Eco Dry (Takara Bio).

Transfection of MBNL2 and mCherry constructs

300 000 HEK293T cells per well were seeded in six-well plates in DMEM (Thermo Fisher Scientific) supplemented with 10% FBS (GenDepot) and 1% Penicillin Streptomycin (Thermo Fisher Scientific) at 37°C in 5% CO_2. The following day, the cells were transfected using Lipofectamine 3000 (Invitrogen). For the pBi-Tet-On vectors, 1 μg of plasmid was co-transfected with 1 μg of a vector expressing rtTA. The following day, expression was induced by switching the media to media containing 1 μg/ml doxycycline (Sigma-Aldrich). The cells were harvested 48 hrs post induction. For the mCherry constructs, 500 ng–1 μg of plasmid was transfected and the cells were harvested 48 hrs post transfection for western blot analysis.

Protein extraction and western blot for cell culture experiments

Cells were scraped from the wells and homogenized in RIPA buffer (Cell Signaling Technology) supplemented with 1× protease inhibitor (GenDepot) and 1× phosphatase inhibitor (GenDepot). The samples were processed, run on 4–20% Criterion TGX Stain-Free Precast Protein Gels (Bio-Rad Laboratories) and transferred as mentioned above. After blocking for 1 hr at room temperature with 5% Blotto Non Fat Dry-Milk (Chem Cruz) in PBST, membranes were probed overnight at 4°C with anti-FLAG (Sigma-Aldrich, M2, 1:2000), anti-Myc (Cell Signaling Technology, 71D10, 1:1000) or anti-vinculin (Sigma-Aldrich, nVIN-1, 1:5000) in 1:1 Odyssey Blocking Buffer PBS (Licor) in PBST. The next day, the blots were washed three times with PBST and incubated for 1 h at RT in secondary antibody. The secondary antibody used to detect anti-Myc was Rabbit IgG (H&L) Antibody DyLight 680 Conjugated (Rockland Immunochemicals; 1:10 000) in 5% non-fat milk in PBST. The secondary antibody used to detect anti-FLAG and anti-vinculin was Mouse IgG (H&L) Antibody DyLight 800 Conjugated (Rockland Immunochemicals; 1:10000) in 5% non-fat milk in PBST. The membranes were washed three times with PBST and then imaged using the Odyssey CLx Imaging System (Licor).

Immunofluorescent staining

300,000 COSM6 cells were seeded onto 35 mm No. 1.5 Coverslip dishes (MATTEK) in DMEM (ThermoFisher Scientific) supplemented with 10% FBS (GenDepot) and 1% Penicillin Streptomycin (ThermoFisher Scientific) at 37°C in 5% CO_2. The same day, the cells were transfected with 1 μg pBi-Tet-On vectors expressing FLAG-MBNL2 and Myc-MBNL2 including (+E6) and/or excluding (–E6) *Mbnl2* exon 6 and 1 μg of a vector expressing rtTA. The following day, expression was induced by switching the media to media containing 1 μg/ml doxycycline (Sigma-Aldrich). Forty eight hours post-inductions, the cells were washed with PBS and fixed in 4% paraformaldehyde. Cells were then blocked in blocking solution (10% FBS, 5% Horse Serum (GenDepot) in PBS with 0.2% Triton X-100 (Sigma-Aldrich)) for 1 h at room temperature. The cells were immunostained with anti-Myc (Cell Signaling Technology, 71D10; 1:250) and anti-FLAG (Sigma-Aldrich, M2; 1:250) antibodies in blocking solution overnight at 4°C. The cells were then washed three times with PBS and incubated with goat anti-Rabbit IgG Alexa Fluor 555 (ThermoFisher Scientific; 1:1500), goat anti-mouse IgG Alexa Fluor 488 (ThermoFisher Scientific; 1:1500), and DAPI (Sigma-Aldrich; 1:2000) for 2 h at room temperature. The cells were washed again three times with PBS and imaged immediately using the Zeiss LSM 880 with Airyscan using laser lines at 405 nm, 488 nm, and 561 nm. Images were analyzed and overlayed using Fiji-2.

Generation of stable cell lines expressing FLAG-MBNL2(+E9) and FLAG-MBNL2(–E9)

Stable C2C12 cell lines expressing FLAG-tagged MBNL2 including (+E9) or excluding exon 9 (–E9) were generated using the pINDUCER system (30). In short, FLAG-MBNL2(+E9) and FLAG-MBNL2(–E9) were amplified using Q5 Hot Start High Fidelity Polymerase (New England Biolabs) and cloned into the pENTR vector (Addgene #22450) digested with NcoI and XhoI (New England Biolabs) using InFusion Snap Assembly Eco Dry (Takara Bio). The inserts were then recombined into the pINDUCER20 vector (Addgene #44012) using Gateway LR Clonase Enzyme (Invitrogen). The correct insertion into the pINDUCER20 vector was confirmed by Sanger sequencing.

For lentiviral production, 5×10^6 HEK239T cells were seeded in a 10 cm dish containing DMEM (Thermo Fisher Scientific) supplemented with 10% FBS (GenDepot) and 1% Penicillin Streptomycin (Thermo Fisher Scientific). The next day, 8 μg of pINDUCER20_FLAG-MBNL2(+E9) or pINDUCER20_FLAG-MBNL2(–E9) vector, 6 μg psPAX2 vector (Addgene #12260) and 2 μg pMD2.G vector (Addgene #12259) were transfected using Lipofectamine 3000 (Invitrogen) according to manufacturer's instructions. The following day, the media was removed and 5 ml of fresh media was added to the dish. The next day, the media was collected and fresh 5 ml of media was added to the dish which was also collected the following day.

For lentiviral transduction of the pINDUCER20_FLAG-MBNL2(+E9) construct, 150 000 C2C12 cells per well were seeded in six-well plates. Twenty-four hours after seeding, 1 ml of the lentiviral-containing media was added to the cells. Due to the low protein expression of FLAG-MBNL2(–E9), the pINDUCER20_FLAG-MBNL2(–E9) virus was first concentrated using the Lenti-X-Concentrator (Takara Bio) according to manufacturer's instructions. 25 000 C2C12 cells per well were seeded in 24-well plates. Twenty-four hours after seeding, all of the concentrated pINDUCER20_FLAG-MBNL2(–E9) virus was added to the cells. The next day, the media was changed to selection media containing DMEM (Thermo Fisher Scientific) supplemented with 10% FBS (GenDepot), 1% Penicillin Streptomycin (Thermo Fisher Scientific) and 1mg/ml InSolution G418 (VWR). The cells were passaged for a minimum of three generations in G418-containing media to ensure complete selection.

Drug treatment of stable cell lines

To test the effect of proteasome and autophagosome inhibitors on in the pINDUCER20_ FLAG-MBNL2(+E9) and pINDUCER20_FLAG-MBNL2(–E9) C2C12 cell lines, 150 000 cells per well were seeded in 6-well plates with DMEM (Thermo Fisher Scientific) supplemented with 10% FBS (GenDepot), 1% Penicillin Streptomycin (Thermo Fisher Scientific) and 1 μg/ml Doxycycline hyclate (Sigma-Aldrich) at 37°C in 5% CO_2 to induce FLAG-MBNL2 expression. Forty-eight hours following cell seeding, the media was removed and fresh media including either 10 μM of the proteasomal inhibitors MG-132 (EMD Millipore), 1 μM of the proteasomal inhibitor Bortezomib (Fisher Scientific) or 1 μM of the autophagosome inhibitor bafilomycin A1 (Cell Signaling Technologies) was added to the cells. The cells were cultured for an additional 10 h and then harvested for western blot analyses.

Statistical analysis

Statistical tests were performed in accordance with the experimental design. Simple comparisons used Student's t-test, whereas multi-group comparisons used one- or two-way ANOVA. In each case, *, **, ***, **** and ns denote $P < 0.05$, $P < 0.01$, $P < 0.001$, $P < 0.0001$ and $P > 0.05$, respectively.

RESULTS

Loss of MBNL1 increases MBNL2 protein but not RNA levels

To investigate the compensatory upregulation of MBNL2 upon MBNL1 loss, we used the CRISPR/Cas9 approach to generate a floxed *Mbnl1* mouse line (C57BL/6NJ) targeting the 1049 bp long exon 3 (Supplemental Figure 1A), which contains the translation start codon. The removal of *Mbnl1* exon 3 was previously shown to ablate MBNL1 protein expression (23,24). Sequencing of the genomic DNA from the F1 founder showed the correct insertion of the LoxP sites (Supplemental Figure 1B). Following backcrossing to C57BL/6NJ wild type mice to remove potential off-target hits, $Mbnl1^{flox/+}$ embryos were incubated with Cre protein and transferred into pseudo-pregnant females to generate germline $Mbnl1^{+/-}$ mice. The resulting mice were genotyped, the recombined allele was confirmed by sequencing for the correct excision of *Mbnl1* exon 3 and the $Mbnl1^{+/-}$ mice were crossed to generate $Mbnl1^{+/+}$ (WT) and $Mbnl1^{-/-}$ mice (Supplemental Figure 1C, D).

Skeletal muscle, heart, and brain tissues were harvested from eight week old WT and $Mbnl1^{-/-}$ mice to measure MBNL1 and MBNL2 protein and RNA levels. We found that the removal of *Mbnl1* exon 3 decreased *Mbnl1* RNA levels by 30–40% and nearly abolished MBNL1 protein expression (Figure 1A-C). Consistent with previous work (7,24), loss of MBNL1 increased MBNL2 protein levels by 2–3-fold in skeletal muscle and heart (Figure 1A, B), while only slightly increasing MBNL2 protein levels in the brain (Figure 1C). In contrast to the upregulation of MBNL2 protein levels, *Mbnl2* mRNA levels were unchanged in the three tissues (Figure 1A–C).

To determine if the compensatory upregulation of MBNL2 is reproducible in another experimental system, we tested the effects of *Mbnl1* knockdown in mouse and human muscle cell lines. Two distinct siRNAs targeting conserved regions in mouse and human *Mbnl1* were used to knock down *Mbnl1* expression in the mouse myoblast C2C12 and the human myoblast LHCN-M2 cell line (31). Both siRNAs significantly reduced *Mbnl1* RNA and protein levels and increased MBNL2 protein levels in differentiated C2C12 and LHCN-M2 cells (Supplemental Figure 2A, B). As observed in mouse tissues, *Mbnl2* RNA levels remained unchanged (Supplemental Figure 2A, B), indicating that the observed upregulation of MBNL2 protein is not due to changes in transcription or mRNA stability.

Taken together, these data show that loss of MBNL1 results in the compensatory upregulation of MBNL2 protein but not RNA levels in skeletal muscle and heart tissues. Interestingly, unlike skeletal muscle and heart, the compensatory upregulation of MBNL2 is not as pronounced in brain tissues. As the compensatory upregulation of MBNL2 is also observed upon siRNA-mediated knockdown of *Mbnl1* in mouse C2C12 and human LHCN-M2 cells, our data suggest that the compensatory mechanism is not restricted to $Mbnl1^{-/-}$ mice but also active in human cells.

Loss of MBNL1 increases the inclusion of *Mbnl2* exon 6 and exon 9

MBNL1 and MBNL2 are RNA-binding proteins involved in the regulation of alternative splicing. To test if loss of MBNL1 affects the splicing of *Mbnl2* mRNA, we scanned *Mbnl2* mRNA for alternative splicing using RT-PCR in skeletal muscle, heart, and brain tissues of WT and $Mbnl1^{-/-}$ mice. We found that loss of MBNL1 moderately increased the inclusion of *Mbnl2* exon 6 (54bp) and exon 9 (95bp) in skeletal muscle and heart (Figure 2A–C), while only slightly affecting the inclusion of both exons in the brain (Figure 2D).

As the compensatory upregulation of MBNL2 was also observed in mouse C2C12 and human LHCN-M2 cell lines, we repeated the RT-PCR for *Mbnl2* exon 6 and exon 9 upon siRNA-mediated knockdown of *Mbnl1* in both cell lines. Similar to what was observed in skeletal muscle and heart, we found that loss of MBNL1 increases the inclusion of *Mbnl2* exon 6 and exon 9 in mouse C2C12 and more so in human LHCN-M2 cells (Supplemental Figure 3A, B).

MBNL proteins typically promote exclusion of an alternative exon via binding to the upstream intron or within the alternative exon (20,32). To investigate if MBNL1 interacts with *Mbnl2* pre-mRNA, we analyzed previously published MBNL1 iCLIP data from C2C12 cells and found that MBNL1 indeed binds upstream and inside *Mbnl2* exon 6 and exon 9 (Supplemental Figure 4) (32), supporting a potential direct effect of MBNL1 on *Mbnl2* splicing.

Together, these data suggest that the splicing of *Mbnl2* exon 6 and exon 9 is under the control of MBNL1 and that the inclusion of the two exons correlate with the increase in MBNL2 protein levels.

Mbnl2 exon 6 regulates the subcellular localization of MBNL2

Mbnl2 exon 6 is homologous to exon 5 of *Mbnl1*, which contains part of a bipartite nuclear localization signal (NLS) (33–35). Similarly, cNLS Mapper predicts that the inclusion of *Mbnl2* exon 6 results in a bipartite NLS (Figure 3A, B) (36). The effect of *Mbnl2* exon 6 inclusion on MBNL2 protein levels and the functionality of the predicted NLS still remain unknown.

To investigate if the enhanced inclusion of *Mbnl2* exon 6 could affect MBNL2 protein levels, we cloned combinations of *Mbnl2* cDNAs including and excluding exon 6 into the doxycycline (dox)-inducible pBi-Tet-On vector, which allows for the comparison of the levels of two *Mbnl2* isoforms expressed from one plasmid under the same promoter (Figure 3C). The pBi-Tet-On vectors were transfected together with a plasmid expressing rtTA into HEK293T cells, and the expression of the constructs was induced using dox for 48 h. The inclusion of *Mbnl2* exon 6 resulted in a size shift of the MBNL2 protein on western blot (Figure 3D).

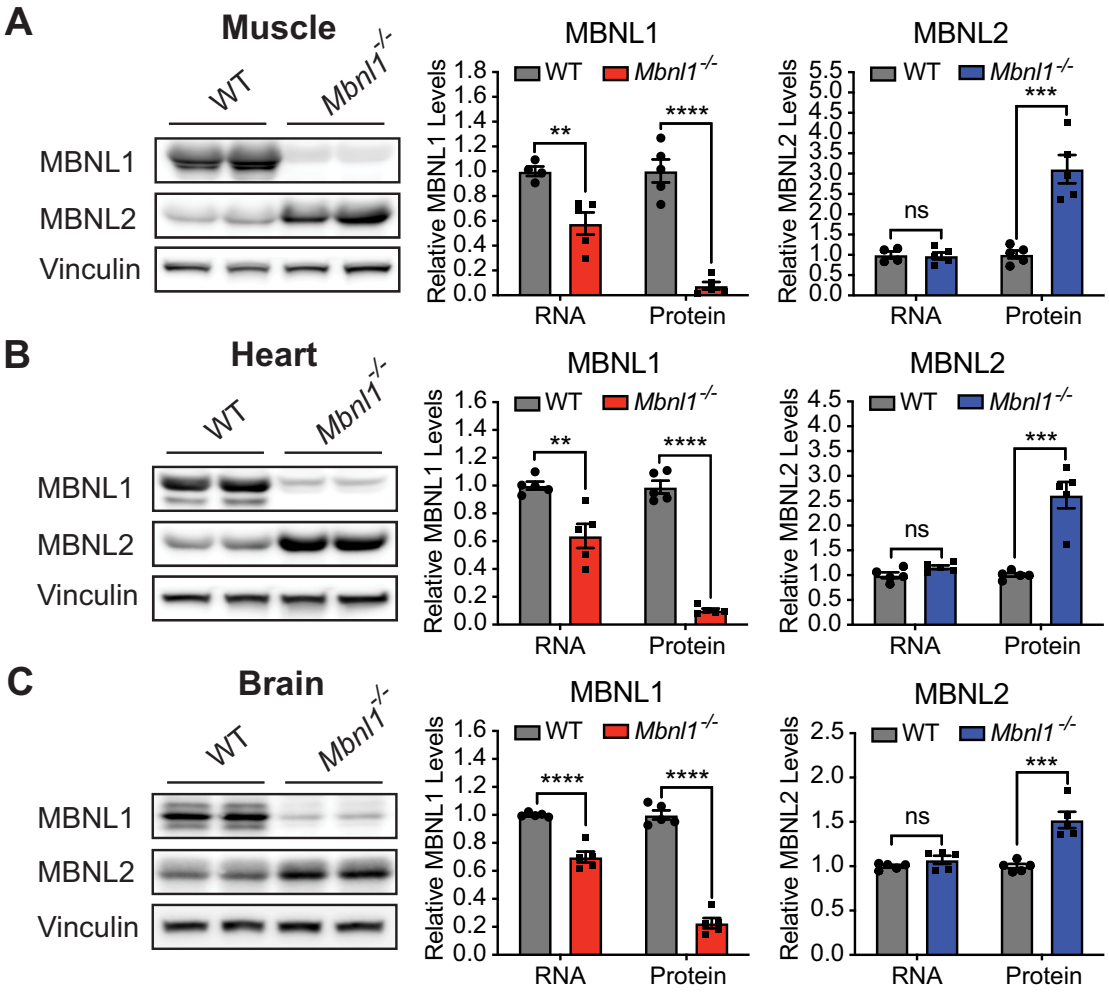

Figure 1. Loss of MBNL1 increases MBNL2 protein but not RNA levels in skeletal muscle, heart and brain. Representative western blot and quantification of MBNL1 and MBNL2 protein and RNA levels in (**A**) skeletal muscle, (**B**) heart and (**C**) brain of *Mbnl1*$^{+/+}$ (WT) and *Mbnl1*$^{-/-}$ mice. For the western blot quantifications, MBNL1 and MBNL2 protein levels were normalized to vinculin. Note that we found that the MBNL1 antibody used cross reacts with MBNL2 (data not shown), which we believe is the residual band in *Mbnl1*$^{-/-}$ tissues. For the RT-qPCR quantifications, *Mbnl1* and *Mbnl2* RNA levels were normalized to *Gapdh*. For each assay, a minimum of four replicates were performed. Simple comparisons used Student's t-test. In each case, **, ***, **** and ns denote $P < 0.01$, $P < 0.001$, $P < 0.0001$ and $P > 0.05$, respectively. All data are represented as means ± SEM.

This observation explains why in certain conditions, such as the siRNA-mediated knockdown of *Mbnl1* in LHCN-M2 cells in which the inclusion of *Mbnl2* exon 6 increases to over 75%, we observe an MBNL2 doublet band (Supplemental Figure 2B, 3B). Importantly, the inclusion of *Mbnl2* exon 6 did not affect MBNL2 protein levels (Figure 3D, Supplemental Figure 5), suggesting that *Mbnl2* exon 6 inclusion is not causative for the increase of MBNL2 protein levels upon loss of MBNL1.

To test if the predicted NLS is functional and the inclusion of *Mbnl2* exon 6 could instead affect the subcellular localization of MBNL2, we transfected the pBi-Tet-On vectors together with a plasmid expressing rtTA in COSM6 cells, which are easy to transfect and contain a large cytoplasmic area that allows for the visualization of MBNL2 localization within the cell. Using immunofluorescent staining, we found that MBNL2 excluding exon 6 is dispersed throughout the cytoplasm and nucleus (Figure 3E; Supplemental Figure 6). As the nuclear pore complex permits relatively unrestrained passage of proteins of up to 60kDa and MBNL2 has a size of around 41 kDa, it is likely that MBNL2 can move freely in and out of the nucleus and is therefore found in both cytoplasm and nucleus (37). Importantly, we further found that the inclusion of *Mbnl2* exon 6 depletes MBNL2 from the cytoplasm, leading to a pronounced nuclear localization (Figure 3E; Supplemental Figure 6).

These data confirm the functionality of the nuclear localization signal in *Mbnl2* exon 6 and are consistent with a previous study showing increased nuclear localization of MBNL2 in *Mbnl1*$^{-/-}$ skeletal muscle (7).

Inclusion of *Mbnl2* exon 9 regulates MBNL2 protein levels

Also the function of *Mbnl2* exon 9 is unknown. Due to its size of 95 bp, the inclusion of exon 9 causes a frameshift,

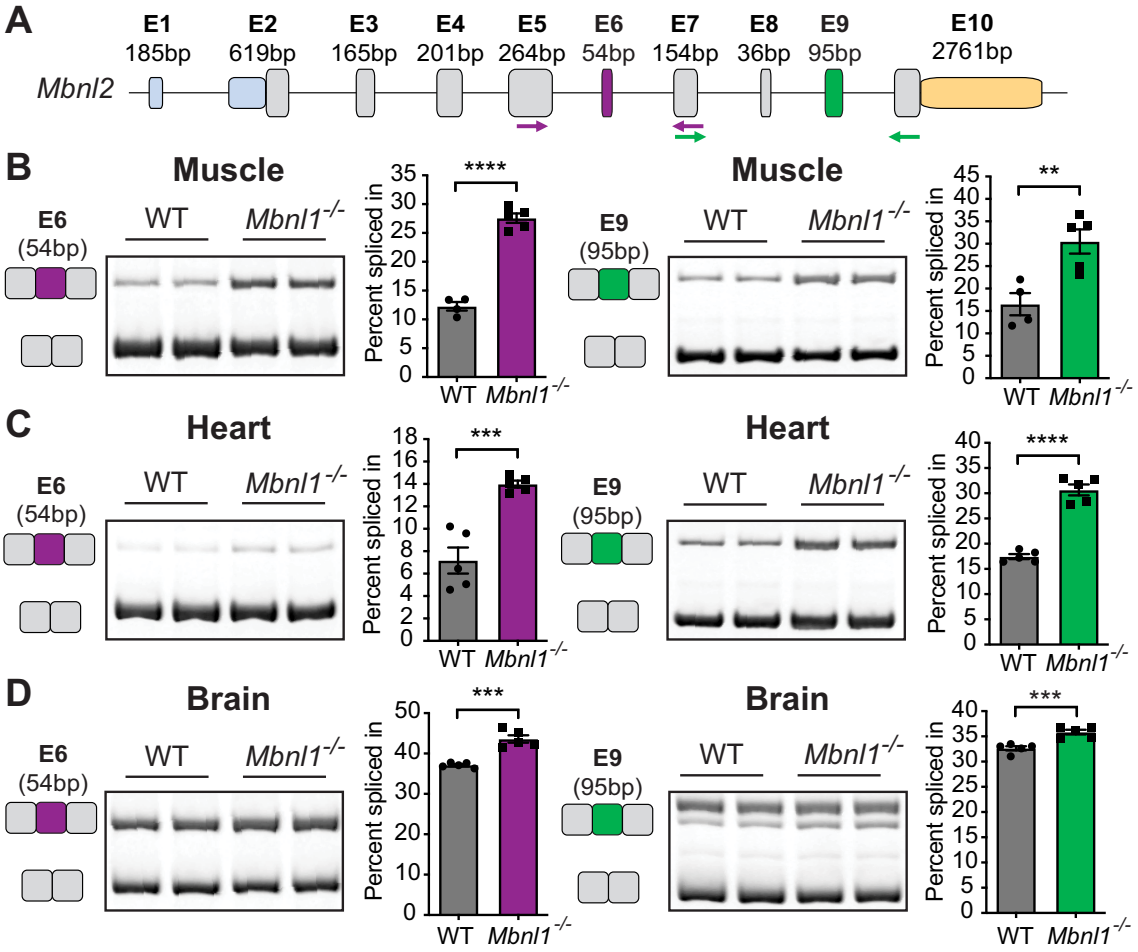

Figure 2. Loss of MBNL1 increases inclusion of *Mbnl2* exon 6 and exon 9 in skeletal muscle, heart and brain. (**A**) Schematic overview of *Mbnl2* exons (5' UTR in blue, protein coding sequence in grey, and 3' UTR in orange) and the location of the primers used to measure splicing of *Mbnl2* exon 6 (E6; purple) and exon 9 (E9; green). Representative polyacrylamide gels showing the inclusion of *Mbnl2* E6 and E9 and quantification of the percent spliced in in the (**B**) skeletal muscle, (**C**) heart and (**D**) brain of $Mbnl1^{+/+}$ (WT) and $Mbnl1^{-/-}$ mice. Note that exon 8 is only expressed in brain but not in skeletal muscle and heart tissues. For each assay, a minimum of four replicates were performed. Simple comparisons used Student's *t*-test. In each case, **, *** and **** denote $P < 0.01$, $P < 0.001$ and $P < 0.0001$, respectively. All data are represented as means ± SEM.

resulting in an alternative C-terminus of MBNL2 (Figure 4A, B).

To investigate if the enhanced inclusion of *Mbnl2* exon 9 could affect MBNL2 protein levels, we cloned combinations of *Mbnl2* cDNAs including and excluding exon 9 into the pBi-Tet-On vector (Figure 4C). The pBi-Tet-On vectors were transfected together with a plasmid expressing rtTA into HEK293T cells and the expression of the constructs was induced using dox for 48 h. Regardless of the placement within the vector, the protein levels of MBNL2 including exon 9 were substantially higher than the levels of MBNL2 lacking exon 9 (Figure 4D, Supplemental Figure 7A). Importantly, RT-PCR analysis demonstrated that the RNA levels of the *Mbnl2* isoform including exon 9 were not higher than the *Mbnl2* isoform excluding exon 9 (Supplemental Figure 7B).

Together, these data indicate that the alternative splicing of *Mbnl2* exon 9 regulates the levels of MBNL2 protein via a mechanism involving translation efficiency or protein stability.

MBNL2 C-terminus resulting from the exclusion of exon 9 destabilizes MBNL2 protein

Upon determining that the splicing of *Mbnl2* exon 9 affects MBNL2 protein levels, we next wanted to investigate the mechanism by which inclusion of *Mbnl2* exon 9 results in higher MBNL2 protein levels. We hypothesized that the inclusion of *Mbnl2* exon 9 could directly increase protein expression via enhanced translation or protein stability. Alternatively, exclusion of *Mbnl2* exon 9 could yield decreased protein levels via reduced translation or protein destabilization. Thus, the inclusion of *Mbnl2* exon 9 and the switch in C-termini could indirectly increase MBNL2 levels by removing a negative regulatory element.

To test these possibilities, we first generated FLAG-mCherry fusion constructs with either the MBNL2 C-terminus including (+E9) or excluding exon 9 (–E9) and expressed them in HEK293T cells (Figure 5A). While the +E9 C-terminus did not affect FLAG-mCherry levels, the –E9 C-terminus drastically reduced FLAG-mCherry levels

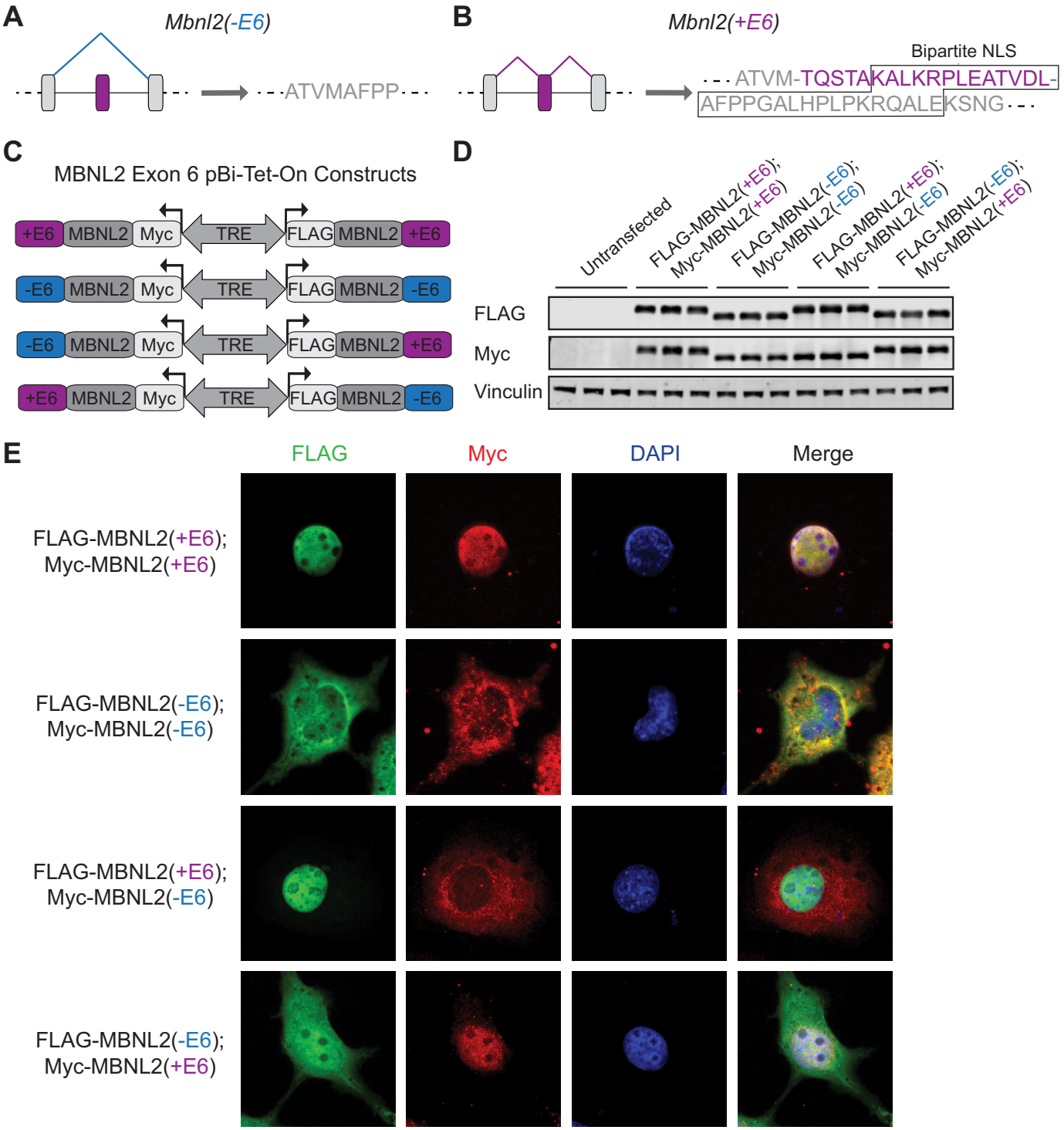

Figure 3. Inclusion of *Mbnl2* exon 6 regulates the subcellular localization of MBNL2. (**A**, **B**) Illustration showing the alternative splicing of *Mbnl2* exon 6 (E6). Inclusion of E6 results in a predicted bipartite nuclear localization signal (NLS). (**C**) Schematic overview of the pBi-Tet-On vectors used to express different combinations of FLAG-MBNL2 and Myc-MBNL2 including (+E6) and excluding exon 6 (–E6). (**D**) Western blots showing the protein levels of FLAG-MBNL2 and Myc-MBNL2 including and excluding E6 upon transfection of the pBi-Tet-On vectors, rtTA vector and induction of expression using 1000 ng/ml dox for 48 h in HEK293T cells. (**E**) Representative immunofluorescent images of single COSM6 cells (magnified from 40×) transfected with pBi-Tet-On constructs expressing MBNL2(+E6) and MBNL2(–E6), rtTA plasmid and induced using 1000 ng/ml dox for 48 h. The cells were stained using DAPI (blue) and anti-FLAG (green) and anti-Myc (red) antibodies.

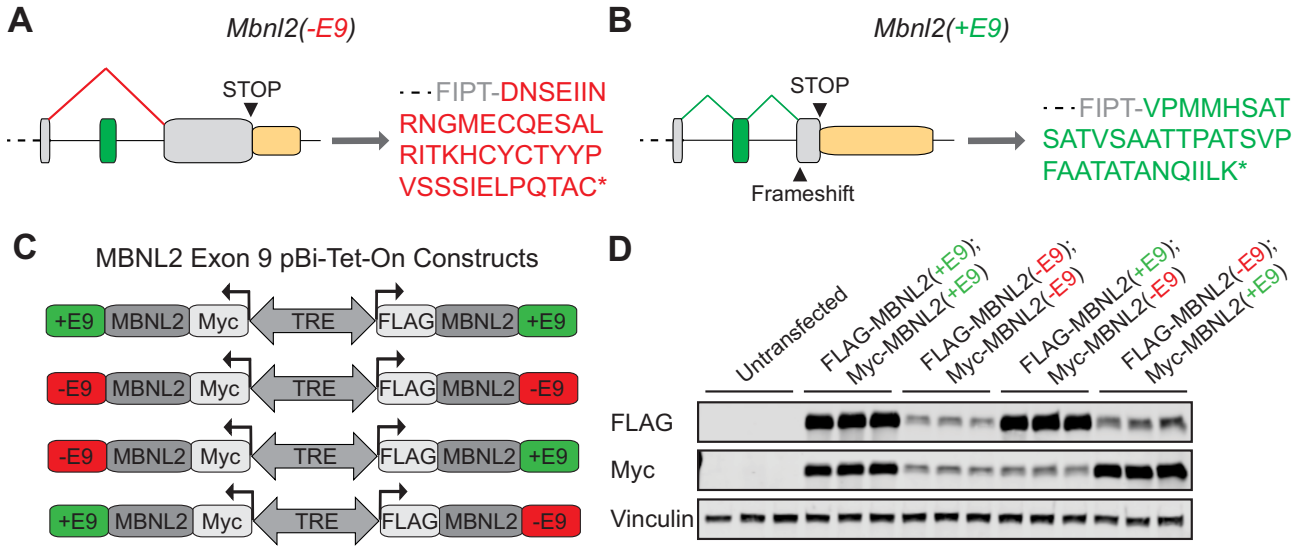

Figure 4. Inclusion of *Mbnl2* exon 9 regulates MBNL2 protein levels. (**A**, **B**) Illustration showing the alternative splicing of *Mbnl2* exon 9 (E9). E9 inclusion results in a frameshift and an alternative MBNL2 C-terminus. (**C**) Schematic overview of the pBi-Tet-On vectors used to express different combinations of FLAG-MBNL2 and Myc-MBNL2 including (+E9) and excluding E9 (–E9). (**D**) Western blots showing the protein levels of FLAG-MBNL2 and Myc-MBNL2 upon transfection of the pBi-Tet-On vectors, rtTA vector and induction of expression using 1000 ng/ml dox for 48 h in HEK293T cells.

(Figure 5A), indicating the presence of a negative regulatory element. To identify the minimal sequence of the negative regulatory element, we used systematic deletion analysis of FLAG-MBNL2 without exon 9 (–E9) using the dox-inducible pBi-Tet-On vector with a Myc-mCherry internal loading control (Figure 5B). Consistent with our previous results, the protein levels of FLAG-MBNL2(–E9) were significantly lower than FLAG-MBNL2(+E9) (Figure 5B). We generated sequential deletions of the –E9 C-terminus in six amino acid (aa) intervals. Deletion of the last six aa drastically increased MBNL2 protein levels (Figure 5B). Deletion of the last 18 aa further increased MBNL2 protein levels, while additional deletions did not lead to a further increase of MBNL2 (Figure 5B), indicating that deletion of the last 18 aa is sufficient to disrupt the negative regulatory element.

Cloning of the last 18 aa as a FLAG-mCherry fusion construct slightly reduced FLAG-mCherry protein levels, but not to a similar extent to the levels of the FLAG-mCherry carrying the complete –E9 C-terminus (Figure 5C), indicating that the last 18 aa are necessary but not sufficient for the full negative regulatory effect.

Lastly, to determine if the mechanism of downregulation is mediated through decreased protein stability rather than an RNA-mediated effect, we introduced stop codon mutations to either remove the entire C-terminal region (Stop 1) or the last 18 aa of the –E9 C-terminus (Stop 2) in our previously generated pBi-Tet-On vectors expressing FLAG-MBNL2 and Myc-mCherry as internal loading control (Figure 5D). In both cases, FLAG-MBNL2 levels were increased to levels comparable to the levels of FLAG-MBNL2(+E9) (Figure 5D), supporting the conclusion that the negative regulatory effect is mediated through the amino acid sequence and a decrease in protein stability.

Together, these data indicate that the –E9 C-terminus negatively regulates MBNL2 levels via a negative regulatory element including the last 18 aa, which destabilizes the MBNL2 protein. The inclusion of *Mbnl2* exon 9 thereby indirectly increases MBNL2 protein levels by altering the MBNL2 C-terminus and removing the negative regulatory domain.

MBNL2 C-terminus excluding exon 9 induces proteasomal degradation

To understand the role of the last 18 aa of the C-terminus excluding exon 9 in regulating MBNL2 protein levels, we applied multiple prediction programs to identify regulatory motifs that fall in the –E9 C-terminus. Using EMBOSS (38), we identified a predicted PEST domain that was not present in the MBNL2 C-terminus including exon 9. The predicted PEST domain spans over the identified 18 aa and is highly conserved among species (Supplemental Figure 8).

PEST domains are negative regulatory domains that are rich in the amino acids proline (P), glutamic acid (E), serine (S) and threonine (T), and are often flanked by positively charged amino acids such as lysine (K), arginine (R) and histidine (H) (39,40). To test if the predicted PEST domain is functional, we cloned the identified PEST domain together with the flanking amino acids as an isolated unit in a FLAG-mCherry fusion construct (Figure 6A). Expression of the FLAG-mCherry fusion construct with the PEST domain in HEK293T cells drastically reduced FLAG-mCherry protein levels to a similar extent to the levels of the FLAG-mCherry(–E9) (Figure 6A), indicating that the PEST domain is sufficient to mediate the negative regulatory effect on MBNL2.

As PEST domains are known to promote the degradation of proteins via the ubiquitin-proteasome pathway (39,40), we next sought to investigate if MBNL2(–E9) is degraded via the proteasome. To test this, we used the pINDUCER20 lentivirus system to generate stable dox-inducible C2C12 cell lines expressing FLAG-MBNL2(+E9)

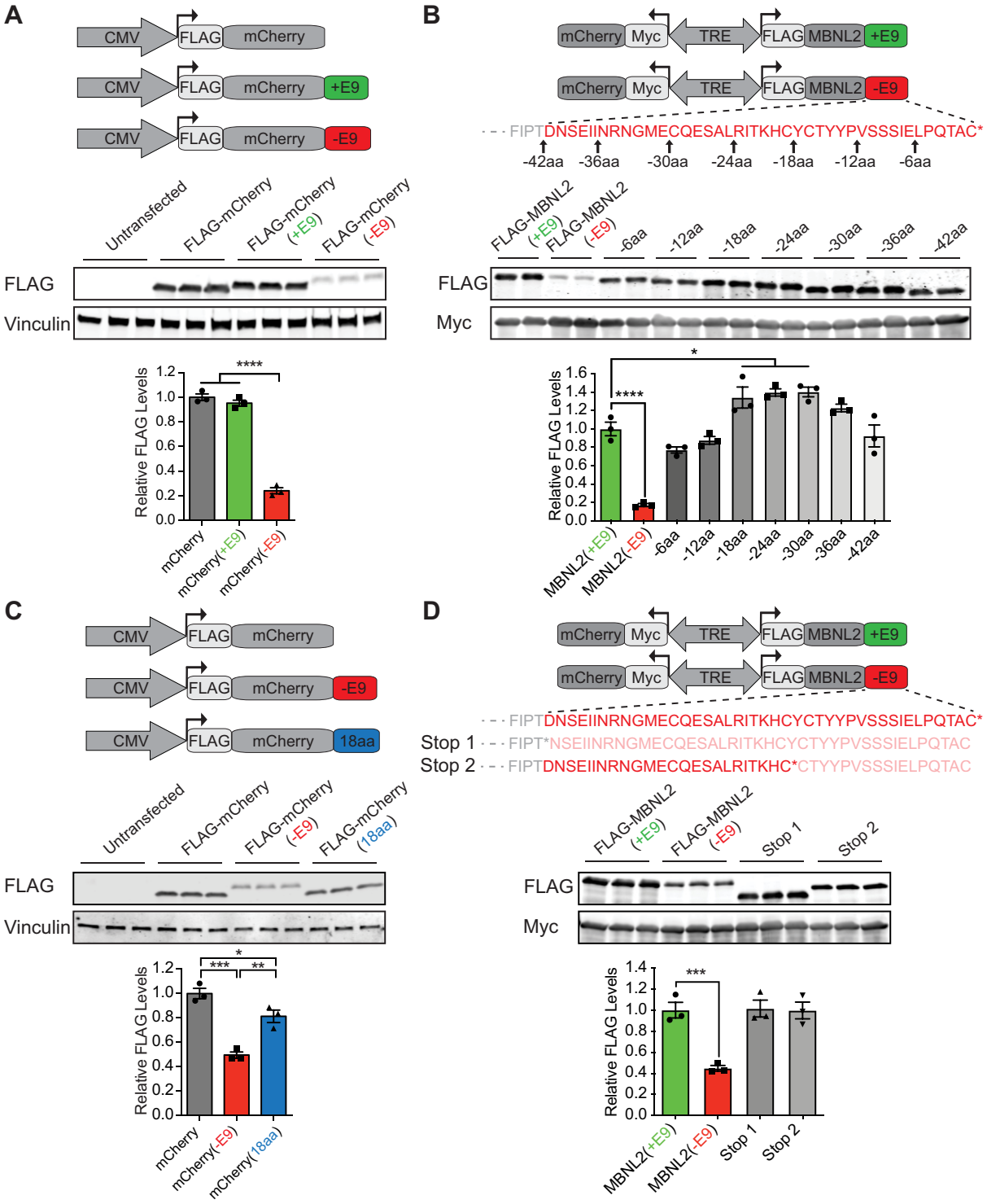

Figure 5. The MBNL2 C-terminus excluding exon 9 destabilizes the MBNL2 protein. Schematic overview of the vectors used to express. (**A**) FLAG-mCherry fusion constructs with either the MBNL2 C-terminus including (+E9) or excluding exon 9 (–E9), (**B**) pBi-Tet-On vectors expressing FLAG-MBNL2(+E9), FLAG-MBNL2(–E9) or FLAG-MBNL2(–E9) with sequential deletions of the C-terminus and Myc-mCherry as internal control, (**C**) FLAG-mCherry fusion constructs with the complete –E9 C-terminus or the last 18aa of the –E9 C-terminus and (**D**) pBi-Tet-On vectors expressing FLAG-MBNL2(+E9), FLAG-MBNL2(–E9) or FLAG-MBNL2(–E9) with stop codon mutations to either remove the entire C-terminal region (Stop 1) or the last 18 aa of the -E9 C-terminus (Stop 2) and Myc-mCherry as internal control. The bidirectional pBi-Tet-On vectors were co-transfected with a rtTA expression plasmid in HEK293T cells and their expression was induced using 1000 ng/ml dox. (A–D) Western blot and quantification showing the protein levels of FLAG-mCherry or FLAG-MBNL2. For the western blot quantifications, FLAG-mCherry levels were normalized to vinculin, while FLAG-MBNL2 levels were normalized to Myc-mCherry. For each assay, a minimum of three replicates were performed. Multi-group comparisons used one-way ANOVA followed by Tukey's multiple comparisons test. In each case, *, **, ***, **** and ns denote $P < 0.05$, $P < 0.01$, $P < 0.001$, $P < 0.0001$ and $P > 0.05$, respectively. All data are represented as means ± SEM.

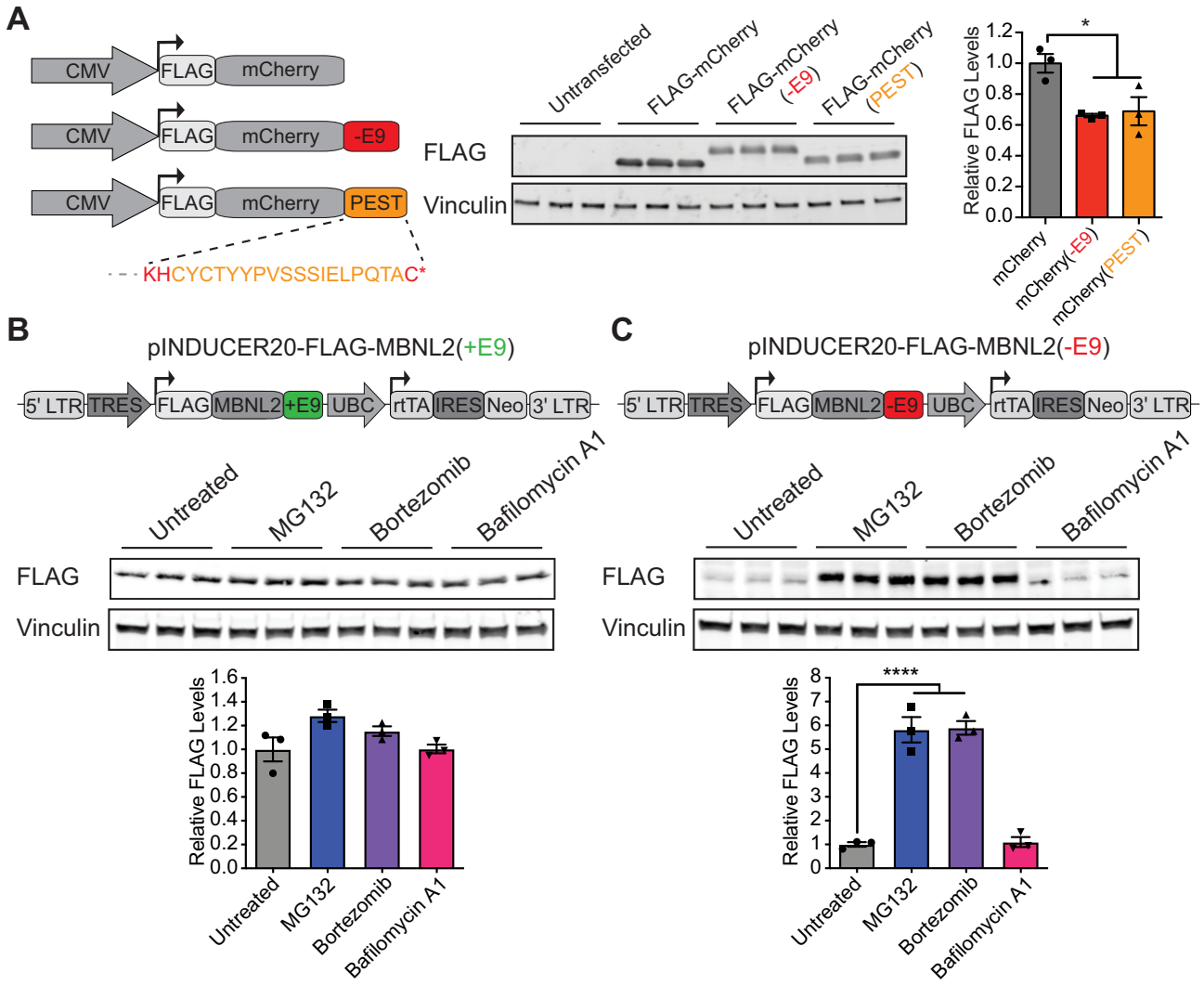

Figure 6. The MBNL2 C-terminus excluding exon 9 induces proteasomal degradation. (**A**) Schematic overview of the vectors used to express FLAG-mCherry fusion constructs with the MBNL2 C-terminus excluding exon 9 (–E9) or the predicted PEST domain. Western blot and quantification of FLAG-mCherry levels. Schematic overview of the pINDUCER20 constructs used to generate stable cell lines expressing (**B**) FLAG-MBNL2(+E9) and (**C**) FLAG-MBNL2(–E9). MBNL2 protein expression was induced using 1000 ng/ml dox for 48 h after which the cells were treated with proteasomal inhibitors MG132 or Bortezomib or the autophagosome inhibitor Bafilomycin A1 for 10 h. Western blot and quantification showing the protein levels of FLAG-MBNL2 in the (B) FLAG-MBNL2(+E9) and (C) FLAG-MBNL2(–E9) cell lines upon inhibitor treatment. For the western blot quantifications, FLAG-mCherry and FLAG-MBNL2 protein levels were normalized to vinculin. For each assay, a minimum of three replicates were performed. Multi-group comparisons used one-way ANOVA followed by Tukey's multiple comparisons test. In each case, * and **** denote $P < 0.05$ and $P < 0.0001$, respectively. All data are represented as means ± SEM.

and FLAG-MBNL2(–E9) to keep the overexpression of the constructs to a minimum (Figure 6B, C) (30). As previously observed, the protein levels of FLAG-MBNL2(+E9) were drastically higher at every tested dox concentration than FLAG-MBNL2(–E9), which was barely detectable on western blot (Supplemental Figure 9). Interestingly, incubation of the cell lines with two different proteasomal inhibitors, MG132 and Bortezomib, drastically increased the protein levels of FLAG-MBNL2(–E9) by 5–6-fold while having no effect on the protein levels of FLAG-MBNL2(+E9) (Figure 6B, C). In contrast, the autophagosome inhibitor Bafilomycin A1 had no effect on the protein levels of either MBNL2 isoform.

We performed ubiquitination assays to compare the extent of ubiquitination of the two MBNL2 isoforms. In agreement with our findings that the MBNL2 isoform excluding exon 9 is highly unstable, we found that the relative ubiquitination level of MBNL2 excluding exon 9 is significantly higher than that of MBNL2 including exon 9 (Supplemental Figure 10).

Together, these data indicate that the -E9 C-terminus contains a negative regulatory PEST domain that promotes MBNL2 degradation via the ubiquitin-proteasome system.

The compensatory mechanism is active in a DM1 mouse model

Loss of MBNL function is the primary disease driver of the multisystemic disorder DM1, in which a CUG repeat

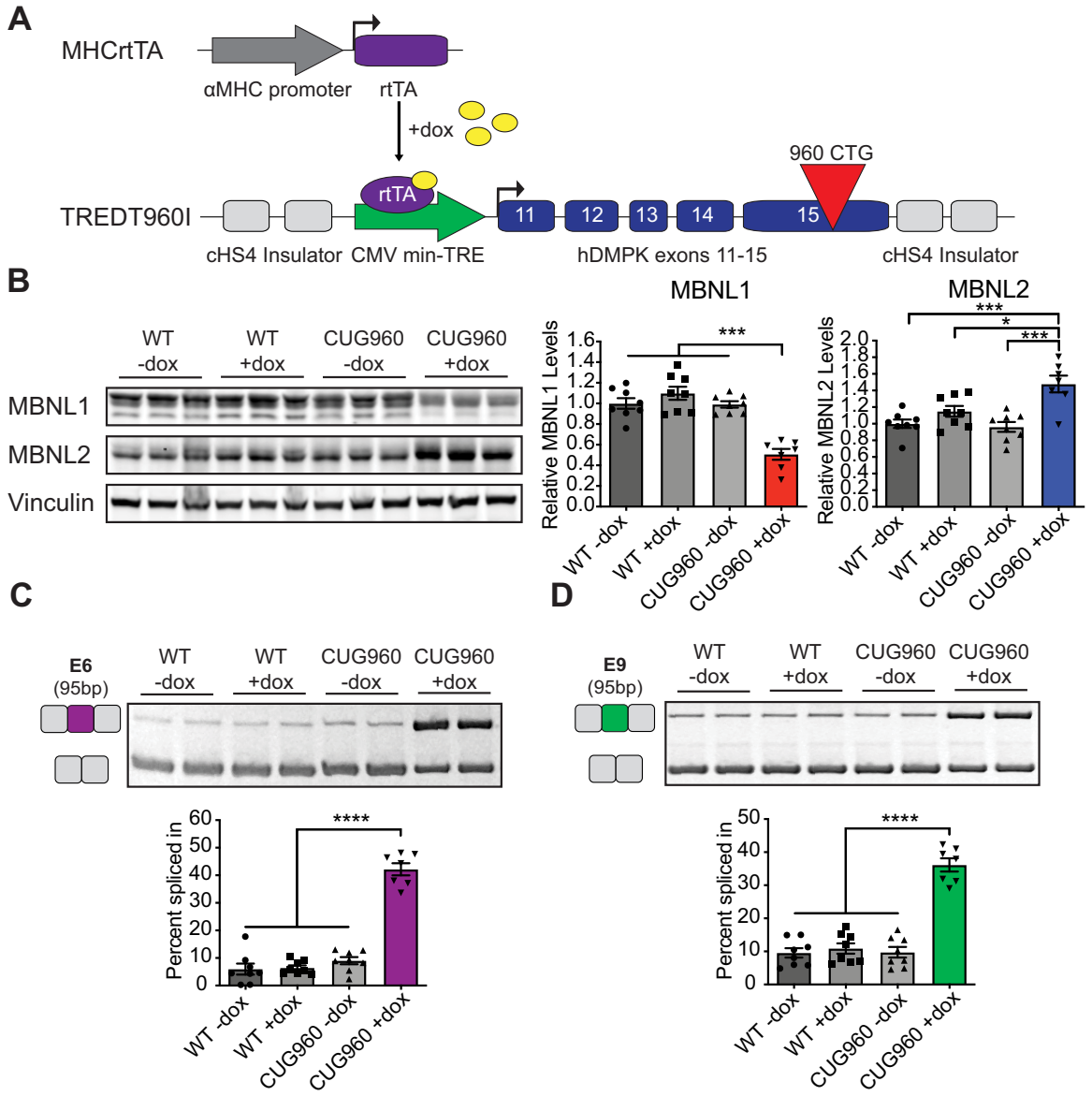

Figure 7. Inclusion of *Mbnl2* exon 6 and exon 9 and MBNL2 protein levels are increased in the CUG960 heart mouse model. (**A**) Schematic overview of the TREDT960I/MHCrtTA (CUG960) heart mouse model. (**B**) Representative western blot and quantification of MBNL1 and MBNL2 protein levels in the heart of WT and CUG960 mice fed on regular chow (-dox) or chow containing 2 g dox/kg (+dox). For the western blot quantification, MBNL1 and MBNL2 protein levels were normalized to vinculin. Representative splicing gel and quantification showing the inclusion of *Mbnl2* (**C**) exon 6 (E6) and (**D**) exon 9 (E9) in WT and CUG960 mice fed on –dox and +dox chow. For each assay, a minimum of seven replicates were performed. Multi-group comparisons used one-way ANOVA followed by Tukey's multiple comparisons test. In each case, *, *** and **** denote $P < 0.05$, $P < 0.001$ and $P < 0.0001$, respectively. All data are represented as means ± SEM.

expansion in the 3' UTR of *DMPK* sequesters the MBNL paralogs causing their loss of function. Thus, we were curious to investigate if the compensatory mechanism also occurs in tissues expressing CUGexp RNA. To do so, we used a recently generated a dox-inducible DM1 heart mouse model (Figure 7A), TREDT960I/MHCrtTA (CUG960), that expresses 960 interrupted CUG repeats in the context of human *DMPK* and recapitulates the electrophysiological and molecular cardiac features of DM1 (25). To test if the inclusion of *Mbnl2* exon 6 and exon 9 and MBNL2 protein levels are increased in heart tissue from these mice, we induced the CUG960 RNA using 2 g dox/kg chow starting at postnatal day 1 and harvested the hearts at eight weeks of age. Similar to what was seen in the *Mbnl1*$^{-/-}$ mice, RT-PCR showed increased inclusion of *Mbnl2* exon 6 and exon 9, while western blot analysis showed that MBNL2 protein levels were significantly increased in the CUG960 mice fed with dox chow (Figure 7B–D). Interestingly, we also observed a reduction of MBNL1 protein levels in the CUG960 mice fed with dox chow (Figure 7B). This observation suggests that expression of the CUG repeat RNA might either downregulate MBNL1 protein levels or that the sequestration of MBNL1 onto the CUG repeat RNA decreases the solubility of MBNL1.

Taken together, these results indicate that MBNL sequestration and loss of function in DM1 also redirects the splicing of *MBNL2* exon 6 and exon 9 and leads to an increase of MBNL2 protein levels in our DM1 heart mouse model. Thus, the compensatory mechanism is likely to be active in DM1 tissues and could function to modify disease severity.

DISCUSSION

In this study, we uncovered the compensatory mechanism by which loss of MBNL1 upregulates the protein levels of its paralog MBNL2. Consistent with previous work (7,24,41), we found that loss of MBNL1 via genetic knockout *in vivo* or siRNA-mediated knockdown in cell culture upregulates MBNL2 protein levels. The increase of MBNL2 protein levels was concomitant with a modest increase in the inclusion of *Mbnl2* exon 9, which results in a frameshift and an alternative MBNL2 C-terminus. We showed that the predominant MBNL2 isoform in heart and muscle, which does not include exon 9, is highly unstable and identified a negative regulatory PEST domain in the –E9 C-terminus that induces protein degradation via the ubiquitin-proteasome system. Loss of MBNL1 thus upregulates MBNL2 levels by increasing the inclusion of *Mbnl2* exon 9, leading to a switch in the C-termini and the removal of the negative regulatory domain. The identified mechanism is reminiscent of the exon skipping event in SMN2 which results in an alternative C-terminus harboring a protein degradation signal that decreases protein stability (42). This exon skipping event is now being targeted via FDA-approved splicing enhancing drugs to increase the SMN2 protein to overcome the loss of SMN1 in Spinal muscular atrophy (SMA).

Intriguingly, we also found that loss of MBNL1 results in a modest increase of the inclusion of *Mbnl2* exon 6, which is predicted to contain part of a bipartite NLS. Similarly, previous studies have shown that MBNL2 has an increased nuclear localization upon loss of MBNL1 (7). In agreement with the results of a previous study (43), we showed that the inclusion of *Mbnl2* exon 6 indeed increases the nuclear localization of MBNL2. Loss of MBNL1, therefore, not only upregulates MBNL2 protein levels via increased inclusion of *Mbnl2* exon 9 by expressing a more stable protein isoform but also increases translocation of MBNL2 to the nucleus via increased inclusion of *Mbnl2* exon 6, further enhancing its ability to compensate for the nuclear functions of MBNL1 as a splicing regulator.

MBNL1 is the predominant paralog in muscle and heart, while MBNL2 is enriched in brain (6,7,20). In this study, we found that the baseline level of inclusion of *Mbnl2* exon 6 and exon 9 in WT mice is lower in muscle and heart tissues than in the brain. The results suggest that in tissues in which MBNL1 levels are high such as the heart and muscle, MBNL1 suppresses the inclusion of *Mbnl2* exon 6 and exon 9 to maintain low MBNL2 protein levels with reduced transport to the nucleus.

Given the similarities of the MBNL paralogs, the question remains if MBNL1 and MBNL3 also contain a splicing-regulated nuclear localization and protein degradation signal. Similar to *Mbnl2* exon 6, also *Mbnl1* contains a 54bp exon which was previously shown to contain a bipartite nuclear localization signal and mediate the localization of MBNL1 to the nucleus (33–35). In contrast, *Mbnl3* does not contain a 54bp exon. Similar to *Mbnl2* exon 9, also *Mbnl1* and *Mbnl3* contain a 95bp exon. Unlike *Mbnl2* exon 9, exclusion of the 95bp exon in MBNL1 results in a short C-terminus that is not predicted to have a PEST domain. The 95bp exon in *Mbnl3* is a constitutive exon that, based on data from the GTEx Portal, is not alternatively spliced, suggesting that MBNL1 and MBNL3 levels are likely not regulated via a splicing-regulated PEST domain similar to the one we identified in MBNL2.

Lastly, we showed that the inclusion of *Mbnl2* exon 6 and exon 9 and MBNL2 protein levels are increased in our recently developed DM1 heart mouse model (25). These data are in concordance with a previous study that also showed an increase in MBNL2 protein levels in another transgenic DM1 heart mouse model (44) and suggests that the compensatory mechanism is active in DM1 tissues.

Previous studies demonstrated that increased expression of MBNL paralogs has disease-modifying effects in various DM animal models, including those expressing expanded CUG repeat RNA (45–48). Thus, in the future it will be of interest to determine the extent to which the compensatory mechanisms counteract DM1 disease and explore if, similar to the splicing-enhancing drugs in SMA, the mechanism could be leveraged for therapeutic purposes. The MBNL paralogs are also sequestered and lose their function in Myotonic Dystrophy Type 2 (DM2), which has similar disease features, pathology, and mechanism as DM1, and in Spinocerebellar Ataxia Type 8 (SCA8) (9,49). Therefore, this study further lays the groundwork to examine the involvement of compensatory mechanism in other repeat expansion disorders.

DATA AVAILABILITY

All data associated with this study are presented in the paper or the Supplementary Data. All other related data, information and materials can be acquired from the corresponding author upon request.

SUPPLEMENTARY DATA

Supplementary Data are available at NAR Online.

ACKNOWLEDGEMENTS

We thank the Genetically Engineered Rodent Models Core (P30CA125123) led by Jason Heaney at Baylor College of Medicine for generation of the floxed *Mbnl1* mouse model. We further thank Drs André Catic and Alessia Calcagni for advice on proteasomal degradation, Dr James Orengo for equipment access, Brandon Nguyen for their help with mouse dissections, and Drs Walid Fakhouri, Ji-Yoen Kim, Jun Young Sonn, James Orengo, Tiemo Klisch, Stephanie Coffin and Eder Xhako for their helpful comments and suggestions.

Author contributions: L.N. and T.A.C. conceived the study, designed experiments, analyzed and interpreted data. L.N. performed the assays and wrote the manuscript. L.N. and T.A.C. edited the manuscript. R.-C.H. and A.N.M. helped with the experimental design and the molecular assays.

L.L. performed immunostaining. All authors reviewed the manuscript and provided input.

FUNDING

National Institutes of Health [R01AR060733 and R01HL147020 to T.A.C.]; Myotonic Dystrophy Foundation [to L.N.]. Funding for open access charge: National Institutes of Health.

Conflict of interest statement. None declared.

REFERENCES

1. Kitano,H. (2004) Biological robustness. *Nat. Rev. Genet.*, **5**, 826–837.
2. Stelling,J., Sauer,U., Szallasi,Z., Doyle,F.J. and Doyle,J. (2004) Robustness of cellular functions. *Cell*, **118**, 675–685.
3. Diss,G., Ascencio,D., Deluna,A. and Landry,C.R. (2014) Molecular mechanisms of paralogous compensation and the robustness of cellular networks. *J. Exp. Zool. Part B Mol. Dev. Evol.*, **322**, 488–499.
4. El-Brolosy,M.A. and Stainier,D.Y.R. (2017) Genetic compensation: a phenomenon in search of mechanisms. *PLoS Genet*., **13**, e1006780.
5. Dandage,R. and Landry,C.R. (2019) Paralog dependency indirectly affects the robustness of human cells. *Mol. Syst. Biol.*, **15**, e8871.
6. Konieczny,P., Stepniak-Konieczna,E. and Sobczak,K. (2014) MBNL proteins and their target rnas, interaction and splicing regulation. *Nucleic Acids Res*., **42**, 10873–10887.
7. Lee,K.Y., Li,M., Manchanda,M., Batra,R., Charizanis,K., Mohan,A., Warren,S.A., Chamberlain,C.M., Finn,D., Hong,H. *et al.* (2013) Compound loss of muscleblind-like function in myotonic dystrophy. *EMBO Mol. Med.*, **5**, 1887–1900.
8. Miller,J.W., Urbinati,C.R., Teng-umnuay,P., Stenberg,M.G., Byrne,B.J., Thornton,C.A. and Swanson,M.S. (2000) Recruitment of human muscleblind proteins to (CUG)n expansions associated with myotonic dystrophy. *EMBO J.*, **19**, 4439–4448.
9. Mankodi,A., Urbinati,C.R., Yuan,Q.P., Moxley,R.T., Sansone,V., Krym,M., Henderson,D., Schalling,M., Swanson,M.S. and Thornton,C.A. (2001) Muscleblind localizes to nuclear foci of aberrant RNA in myotonic dystrophy types 1 and 2. *Hum. Mol. Genet.*, **10**, 2165–2170.
10. Harper,P. and Johnson,K. (2001) Myotonic Dystrophy | The Online Metabolic and Molecular Bases of Inherited Disease | OMMBID | McGraw-Hill Medical. In.
11. Turner,C. and Hilton-Jones,D. (2010) The myotonic dystrophies: diagnosis and management. *J. Neurol. Neurosurg. Psychiatry*, **81**, 358–367.
12. Brook,J.D., McCurrach,M.E., Harley,H.G., Buckler,A.J., Church,D., Aburatani,H., Hunter,K., Stanton,V.P., Thirion,J.P., Hudson,T. *et al.* (1992) Molecular basis of myotonic dystrophy: expansion of a trinucleotide (CTG) repeat at the 3′ end of a transcript encoding a protein kinase family member. *Cell*, **68**, 799–808.
13. Mahadevan,M., Tsilfidis,C., Sabourin,L., Shutler,G., Amemiya,C., Jansen,G., Neville,C., Narang,M., Barceló,J., O'Hoy,K. *et al.* (1992) Myotonic dystrophy mutation: an unstable CTG repeat in the 3′ untranslated region of the gene. *Science*, **255**, 1253–1255.
14. Fu,Y.H., Pizzuti,A., Fenwick,R.G., King,J., Rajnarayan,S., Dunne,P.W., Dubel,J., Nasser,G.A., Ashizawa,T., De Jong,P. *et al.* (1992) An unstable triplet repeat in a gene related to myotonic muscular dystrophy. *Science*, **255**, 1256–1258.
15. De Temmerman,N., Sermon,K., Seneca,S., De Rycke,M., Hilven,P., Lissens,W., Van Steirteghem,A. and Liebaers,I. (2004) Intergenerational instability of the expanded CTG repeat in the DMPK gene: studies in human gametes and preimplantation embryos. *Am. J. Hum. Genet.*, **75**, 325–329.
16. Morales,F., Couto,J.M., Higham,C.F., Hogg,G., Cuenca,P., Braida,C., Wilson,R.H., Adam,B., Del Valle,G., Brian,R. *et al.* (2012) Somatic instability of the expanded CTG triplet repeat in myotonic dystrophy type 1 is a heritable quantitative trait and modifier of disease severity. *Hum. Mol. Genet.*, **21**, 3558–3567.
17. Tomé,S. and Gourdon,G. (2020) DM1 phenotype variability and triplet repeat instability: challenges in the development of new therapies. *Int. J. Mol. Sci.*, **21**, 457.
18. Jiang,H., Mankodi,A., Swanson,M.S., Moxley,R.T. and Thornton,C.A. (2004) Myotonic dystrophy type 1 is associated with nuclear foci of mutant RNA, sequestration of muscleblind proteins and deregulated alternative splicing in neurons. *Hum. Mol. Genet.*, **13**, 3079–3088.
19. Oddo,J.C., Saxena,T., McConnell,O.L., Berglund,J.A. and Wang,E.T. (2016) Conservation of context-dependent splicing activity in distant Muscleblind homologs. *Nucleic Acids Res*., **44**, 8352–8362.
20. Charizanis,K., Lee,K.Y., Batra,R., Goodwin,M., Zhang,C., Yuan,Y., Shiue,L., Cline,M., Scotti,M.M., Xia,G. *et al.* (2012) Muscleblind-like 2-Mediated alternative splicing in the developing brain and dysregulation in myotonic dystrophy. *Neuron*, **75**, 437–450.
21. Kanadia,R.N., Urbinati,C.R., Crusselle,V.J., Luo,D., Lee,Y.J., Harrison,J.K., Oh,S.P. and Swanson,M.S. (2003) Developmental expression of mouse muscleblind genes Mbnl1, Mbnl2 and Mbnl3. *Gene Expr. Patterns*, **3**, 459–462.
22. Spruce,T., Plass,M., Gohr,A., Ray,D., de Lagrán,M.M., Rot,G., Nóvoa,A., Burguera,D., Permanyer,J., Miret,M. *et al.* (2022) The X-linked splicing regulator MBNL3 has been co-opted to restrict placental growth in eutherians. *PLoS Biol*., **20**, e3001615.
23. Kanadia,R.N., Johnstone,K.A., Mankodi,A., Lungu,C., Thornton,C.A., Esson,D., Timmers,A.M., Hauswirth,W.W. and Swanson,M.S. (2003) A muscleblind knockout model for myotonic dystrophy. *Science (80-.)*., **302**, 1978–1980.
24. Dixon,D.M., Choi,J., El-Ghazali,A., Park,S.Y., Roos,K.P., Jordan,M.C., Fishbein,M.C., Comai,L. and Reddy,S. (2015) Loss of muscleblind-like 1 results in cardiac pathology and persistence of embryonic splice isoforms. *Sci. Rep.*, **5**, 9042.
25. Rao,A.N., Campbell,H.M., Guan,X., Word,T.A., Wehrens,X.H.T., Xia,Z. and Cooper,T.A. (2021) Reversible cardiac disease features in an inducible CUG repeat RNA–expressing mouse model of myotonic dystrophy. *JCI Insight*, **6**, e143465.
26. Yang,H., Wang,H. and Jaenisch,R. (2014) Generating genetically modified mice using CRISPR/Cas-mediated genome engineering. *Nat. Protoc.*, **9**, 1956–1968.
27. Richardson,C.D., Ray,G.J., DeWitt,M.A., Curie,G.L. and Corn,J.E. (2016) Enhancing homology-directed genome editing by catalytically active and inactive CRISPR-Cas9 using asymmetric donor DNA. *Nat. Biotechnol.*, **34**, 339–344.
28. Hodgkins,A., Farne,A., Perera,S., Grego,T., Parry-Smith,D.J., Skarnes,W.C. and Iyer,V. (2015) WGE: a CRISPR database for genome engineering. *Bioinformatics*, **31**, 3078–3080.
29. Kim,K., Kim,H. and Lee,D. (2009) Site-specific modification of genome with cell-permeable cre fusion protein in preimplantation mouse embryo. *Biochem. Biophys. Res. Commun.*, **388**, 122–126.
30. Meerbrey,K.L., Hu,G., Kessler,J.D., Roarty,K., Li,M.Z., Fang,J.E., Herschkowitz,J.I., Burrows,A.E., Ciccia,A., Sun,T. *et al.* (2011) The pINDUCER lentiviral toolkit for inducible RNA interference in vitro and in vivo. *Proc. Natl. Acad. Sci. U.S.A.*, **108**, 3665–3670.
31. Zhu,C.H., Mouly,V., Cooper,R.N., Mamchaoui,K., Bigot,A., Shay,J.W., Di Santo,J.P., Butler-Browne,G.S. and Wright,W.E. (2007) Cellular senescence in human myoblasts is overcome by human telomerase reverse transcriptase and cyclin-dependent kinase 4: consequences in aging muscle and therapeutic strategies for muscular dystrophies. *Aging Cell*, **6**, 515–523.
32. Wang,E.T., Cody,N.A.L., Jog,S., Biancolella,M., Wang,T.T., Treacy,D.J., Luo,S., Schroth,G.P., Housman,D.E., Reddy,S. *et al.* (2012) Transcriptome-wide regulation of pre-mRNA splicing and mRNA localization by muscleblind proteins. *Cell*, **150**, 710–724.
33. Terenzi,F. and Ladd,A.N. (2010) Conserved developmental alternative splicing of muscleblind-like (MBNL) transcripts regulates MBNL localization and activity. *RNA Biol.*, **7**, 43–55.
34. Tran,H., Gourrier,N., Lemercier-Neuillet,C., Dhaenens,C.M., Vautrin,A., Fernandez-Gomez,F.J., Arandel,L., Carpentier,C., Obriot,H., Eddarkaoui,S. *et al.* (2011) Analysis of exonic regions involved in nuclear localization, splicing activity, and dimerization of muscleblind-like-1 isoforms. *J. Biol. Chem.*, **286**, 16435–16446.
35. Lin,X., Miller,J.W., Mankodi,A., Kanadia,R.N., Yuan,Y., Moxley,R.T., Swanson,M.S. and Thornton,C.A. (2006) Failure of MBNL1-dependent post-natal splicing transitions in myotonic dystrophy. *Hum. Mol. Genet.*, **15**, 2087–2097.
36. Kosugi,S., Hasebe,M., Tomita,M. and Yanagawa,H. (2009) Systematic identification of cell cycle-dependent yeast

nucleocytoplasmic shuttling proteins by prediction of composite motifs. *Proc. Natl. Acad. Sci. U.S.A.*, **106**, 10171–10176.
37. Weis,K. (2003) Regulating access to the genome: nucleocytoplasmic transport throughout the cell cycle. *Cell*, **112**, 441–451.
38. Rice,P., Longden,L. and Bleasby,A. (2000) EMBOSS: the European Molecular Biology Open Software Suite. *Trends Genet.*, **16**, 276–277.
39. Rogers,S., Wells,R. and Rechsteiner,M. (1986) Amino acid sequences common to rapidly degraded proteins: the PEST hypothesis. *Science*, **234**, 364–368.
40. García-Alai,M.M., Gallo,M., Salame,M., Wetzler,D.E., McBride,A.A., Paci,M., Cicero,D.O. and De Prat-Gay,G. (2006) Molecular basis for phosphorylation-dependent, PEST-mediated protein turnover. *Structure*, **14**, 309-319.
41. Wang,E.T., Treacy,D., Eichinger,K., Struck,A., Estabrook,J., Olafson,H., Wang,T.T., Bhatt,K., Westbrook,T., Sedehizadeh,S. *et al.* (2019) Transcriptome alterations in myotonic dystrophy skeletal muscle and heart. *Hum. Mol. Genet.*, **28**, 1312–1321.
42. Cho,S. and Dreyfuss,G. (2010) A degron created by SMN2 exon 7 skipping is a principal contributor to spinal muscular atrophy severity. *Genes Dev.*, **24**, 438-442.
43. Sznajder,L.J., Michalak,M., Taylor,K., Cywoniuk,P., Kabza,M., Wojtkowiak-Szlachcic,A., Matłłoka,M., Konieczny,P. and Sobczak,K. (2016) Mechanistic determinants of MBNL activity. *Nucleic Acids Res.*, **44**, 10326–10342.
44. Tylock,K.M., Auerbach,D.S., Tang,Z.Z., Thornton,C.A. and Dirksen,R.T. (2020) Biophysical mechanisms for QRS- And QTc-interval prolongation in mice with cardiac expression of expanded CUG-repeat RNA. *J. Gen. Physiol.*, **152**, e201912450.
45. Kanadia,R.N., Shin,J., Yuan,Y., Beattie,S.G., Wheeler,T.M., Thornton,C.A. and Swanson,M.S. (2006) Reversal of RNA missplicing and myotonia after muscleblind overexpression in a mouse poly(CUG) model for myotonic dystrophy. *Proc. Natl. Acad. Sci. U.S.A.*, **103**, 11748–11753.
46. Chamberlain,C.M. and Ranum,L.P.W. (2012) Mouse model of muscleblind-like 1 overexpression: skeletal muscle effects and therapeutic promise. *Hum. Mol. Genet.*, **21**, 4645–4654.
47. Bargiela,A., Sabater-Arcis,M., Espinosa-Espinosa,J., Zulaica,M., De Munain,A.L. and Artero,R. (2019) Increased muscleblind levels by chloroquine treatment improve myotonic dystrophy type 1 phenotypes in in vitro and in vivo models. *Proc. Natl. Acad. Sci. U.S.A.*, **116**, 25203–25213.
48. Overby,S.J., Cerro-Herreros,E., González-Martínez,I., Varela,M.A., Seoane-Miraz,D., Jad,Y., Raz,R., Møller,T., Pérez-Alonso,M., Wood,M.J. *et al.* (2022) Proof of concept of peptide-linked blockmiR-induced MBNL functional rescue in myotonic dystrophy type 1 mouse model. *Mol. Ther.Nucleic Acids*, **27**, 1146–1155.
49. Daughters,R.S., Tuttle,D.L., Gao,W., Ikeda,Y., Moseley,M.L., Ebner,T.J., Swanson,M.S. and Ranum,L.P.W. (2009) RNA gain-of-function in spinocerebellar ataxia type 8. *PLoS Genet.*, **5**, e1000600.